Acta Mech 223, 81–93 (2012)
DOI 10.1007/s00707-011-0551-6

Y. Heydarpour · P. Malekzadeh · M. R. Golbahar Haghighi · M. Vaghefi

Thermoelastic analysis of rotating laminated functionally graded cylindrical shells using layerwise differential quadrature method

Received: 23 May 2011 / Published online: 21 September 2011

Abstract An accurate and efficient solution procedure based on the elasticity theory is employed to investigate the thermoelastic behavior of rotating laminated functionally graded (FG) cylindrical shells in thermal environment. The material properties are assumed to be temperature dependent and graded in the thickness direction. In order to accurately model the variation of the field variables across the thickness, the shell is divided into a set of mathematical layers. The differential quadrature method (DQM) is adopted to discretize the governing differential equations of each layer together with the related boundary and compatibility conditions at the interface of two adjacent layers. Using the DQM enables one to accurately and efficiently discretize the partial differential equations, especially along the graded direction, and also implement the boundary and compatibility conditions in their strong forms. After demonstrating the convergence and accuracy of the presented approach, the effects of material and geometrical parameters and also temperature dependence of material properties on the stresses and displacement components of rotating laminated FG cylindrical shells are studied.

1 Introduction

Rotating functionally graded (FG) cylindrical shells are increasingly being used in many engineering applications like aviation, rocketry, missiles, chemical, aero-space, and mechanical industries. Functionally graded materials (FGMs) are usually made of a mixture of ceramic and metals. The ceramic constituent of the material provides the high temperature resistance due to its low thermal conductivity. The ductile metal constituent, on the other hand, prevents fracture caused by stress due to a high temperature gradient. These materials are mainly constructed to operate in high temperature environments. Hence, accurate prediction of the induced stresses and deformations based on a thermoelastic analysis are essential for their engineering design and manufacture.

The thermoelastic analysis of non-rotating FG cylindrical shells has been extensively studied; see for example Refs. [1–3]. Also, there have been some research works on the thermoelastic analysis of FG rotating disks based on elasticity or plate theories [4–10]. However, there exist only few studies concerned with the elastic or thermoelastic analysis of FG rotating cylindrical shells [11–13].

Zenkour et al. [11] developed analytical solutions for rotating functionally graded hollow and solid long cylinders based on the plane strain assumption. Young's modulus and material density of the cylinder were assumed

Y. Heydarpour (✉) · P. Malekzadeh · M. R. Golbahar Haghighi
Department of Mechanical Engineering, Persian Gulf University, Bushehr 75168, Iran
E-mail: yasin_heydarpour@yahoo.com; heydarpour.y@gmail.com
Tel.: +98-771-4222150
Fax: +98-771-4540376

M. Vaghefi
Department of Civil Engineering, Persian Gulf University, Bushehr 75168, Iran

to vary exponentially in the radial direction. In addition, a viscoelastic solution to the rotating viscoelastic cylinder was presented, and the dependence of stresses in hollow and solid cylinders on the time parameter was examined. Zamani Nejad and Rahimi [12] studied stresses in rotating thick-walled FG cylindrical shells using elasticity theory subjected to plane stress and strain conditions. Material properties vary in the radial direction according to a power law. Khorshidvand and Khalili [13] presented an analytical solution for the one-dimensional mechanical and thermal stresses in an FG rotating thick cylinder. They assumed that the material properties vary exponentially through the thickness of the shell. In all of these works, constant Poisson's ratio was used.

In all of these works, single-layer FG cylindrical shells with temperature-independent material properties based on one-dimensional theories were considered. Consequently, the axial variations of the field variables were neglected, and only the radial variation of the field variables was considered. These motivate us to study the thermoelastic behavior of rotating multilayered FG cylindrical shells with the temperature-dependent material properties based on the two-dimensional elasticity theory. A layerwise approach together with the differential quadrature method (DQM) [14–19] is employed to discretize the governing thermoelastic equations. The effect of angular velocity, thickness-to-outer radius and length ratios, material properties, and the convection heat transfer coefficient of inside hot fluid on the displacement and stress components are investigated.

2 Mathematical modeling

Consider a multi-layered FG cylindrical shell composed of N_L perfectly bonded physical layers and rotating about its axis with a constant angular velocity Ω (Fig. 1). The material properties and thickness of each layer of

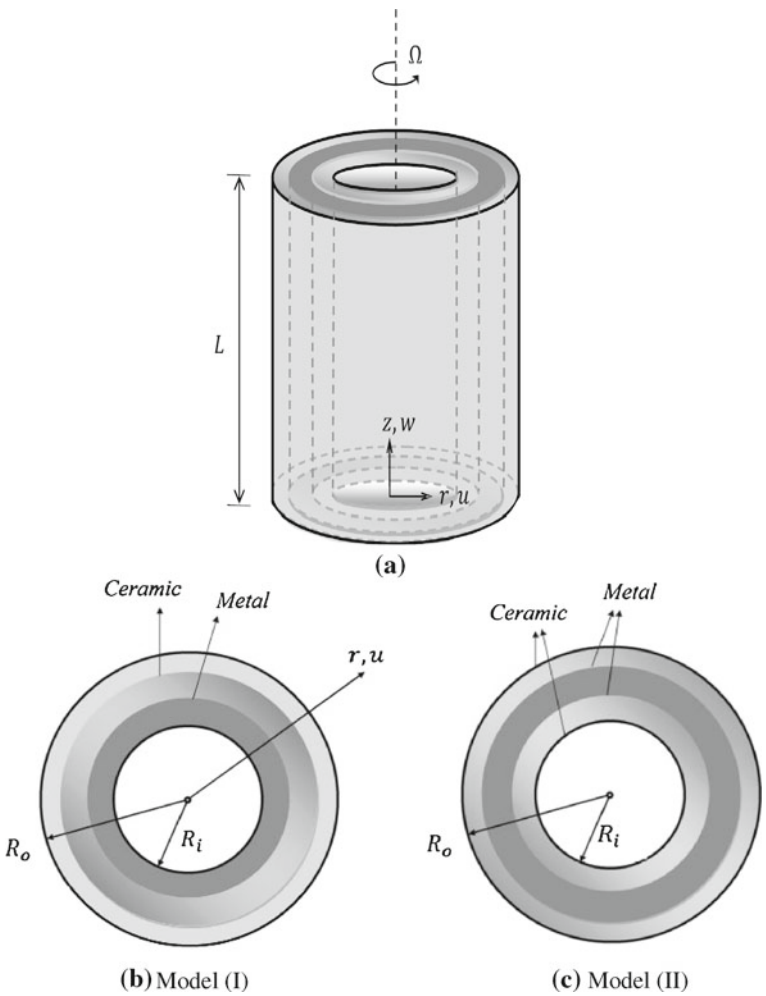

Fig. 1 Geometry of laminated FG cylindrical shell

the shell are assumed to be arbitrary. Also, it is assumed that a hot fluid with uniform temperature moves inside the cylinder. Due to axisymmetric geometry and loading condition of the shell, an axisymmetric deformation results in it. Hence, a cylindrical coordinate system (r, z) is sufficient to label the material points of the cylinder in the undeformed reference configuration. The displacement components of an arbitrary material point of the cylinder are denoted as u and w in the r and z direction, respectively.

The material properties of each layer of the shell vary continuously and smoothly in the thickness direction r according to the power law distribution such that the inner (outer) surface of each layer is ceramic rich (metal rich) and the outer surface is metal rich (ceramic rich). Hence, a typical effective material property 'P' of the eth layer can be represented as

$$P^e(r, T) = P_a^e(T) + \left[P_b^e(T) - P_a^e(T)\right]\left(\frac{r - R_i^e}{R_o^e - R_i^e}\right)^p. \tag{1}$$

If the inner surface of the layer is metal rich then $a = m$ and $b = c$ otherwise, if the inner surface is ceramic rich then $a = c$ and $b = m$, where subscripts m and c refer to the metal and ceramic constituents, respectively; p is the power law index (or the material property graded index); T is the temperature (in Kelvin) at an arbitrary material point of the cylinder; R_i^e and R_o^e are the inner and outer radius of the eth layer, respectively. Hereafter, a superscript 'e' denotes the properties and field variables of the eth layer.

The temperature dependence of a typical material property 'Q^e' of the eth layer can be represented as [20]

$$Q^e(T) = Q_0^e\left(Q_{-1}^e T^{-1} + 1 + Q_1^e T + Q_2^e T^2 + Q_3^e T^3\right). \tag{2}$$

The coefficients $Q_i^e (i = -1, 0, 1, 2, 3)$ are unique to the constituent materials.

In order to accurately model the thermoelastic behavior of the shell, it is divided into N_e mathematical layers, the number of which may be equal to the number of physical layers N_L. In the following, the governing equations of each mathematical layer of the shell are presented.

It is assumed that the shell is stress free at the temperature T_0 and the temperature rise is uniform or varies across its thickness and no heat generation source exists within it. Hence, the temperature distribution along the thickness direction can be obtained by solving the following steady-state one-dimensional heat transfer equation in each layer of the cylinder:

$$\frac{1}{r}\frac{d}{dr}\left(rK^e\frac{dT^e}{dr}\right) = 0 \tag{3}$$

where K^e is the thermal conductivity of the eth layer. Different thermal boundary conditions can be considered at the inner and the outer surfaces of the shell. Without loss of generality, the following thermal boundary conditions are considered at the inner and outer surfaces of the shell, respectively:

$$\underline{-K^1(r, T)\frac{dT^e}{dr} = h\left(T_\infty - T^1\right)} \quad \text{at} \quad r = R_i^1 \quad \text{and} \quad T^{N_e} = T_0 \quad \text{at} \quad r = R_o^{N_e} \tag{4.1, 2}$$

where T_∞ and h are the inside hot fluid temperature and the convection heat transfer coefficient, respectively.

In addition, at the interface of two adjacent layers, one should satisfy the following conditions:

$$T\left(R_o^e\right) = T\left(R_i^{e+1}\right), \quad \underline{\left[K^e(r, T)\frac{dT^e}{dr}\right]_{r=R_o^e} = \left[K^{e+1}(r, T)\frac{dT^{e+1}}{dr}\right]_{r=R_i^{e+1}}}. \tag{5.1, 2}$$

Due to steady-state axisymmetric thermo-mechanical loading conditions, the thermoelastic governing equations of each layer become steady state and axisymmetric. Under these conditions, the governing equations are presented in the following.

The constitutive relations based on the three-dimensional elasticity theory become

$$\underline{\begin{Bmatrix}\sigma_{rr}^e\\ \sigma_{\theta\theta}^e\\ \sigma_{zz}^e\\ \sigma_{rz}^e\end{Bmatrix} = \begin{bmatrix}C_{11}^e & C_{12}^e & C_{13}^e & 0\\ C_{12}^e & C_{22}^e & C_{23}^e & 0\\ C_{13}^e & C_{23}^e & C_{33}^e & 0\\ 0 & 0 & 0 & C_{55}^e\end{bmatrix}\begin{Bmatrix}\varepsilon_{rr}^e - \varepsilon_T^e\\ \varepsilon_{\theta\theta}^e - \varepsilon_T^e\\ \varepsilon_{zz}^e - \varepsilon_T^e\\ 2\varepsilon_{rz}^e\end{Bmatrix}}, \quad \underline{-\varepsilon_T^e = \int_{T_0}^{T}\alpha^{(e)}dT} \tag{6.1, 2}$$

Table 1 Temperature-dependent coefficients of material properties for ceramic (ZrO_2) and metals (Ti-6Al-4V) [20]

	Material	Q_{-1}	Q_0	Q_1	Q_2	Q_3
E	Ti-6Al-4V	0	122.7 (GPa)	-4.605×10^{-4}	0	0
	ZrO_2	0	132.2 (GPa)	-3.805×10^{-4}	-6.127×10^{-8}	0
ν	Ti-6Al-4V	0	0.2888	1.108×10^{-4}	0	0
	ZrO_2	0	0.3330	0	0	0
ρ	Ti-6Al-4V	0	4420 (kg/m^3)	0	0	0
	ZrO_2	0	3657 (kg/m^3)	0	0	0
α	Ti-6Al-4V	0	7.43×10^{-6}(1/K)	7.483×10^{-4}	-3.621×10^{-7}	0
	ZrO_2	0	13.3×10^{-6}(1/K)	-1.421×10^{-3}	9.549×10^{-7}	0
k	Ti-6Al-4V	0	6.10 (W/mK)	0	0	0
	ZrO_2	0	1.78 (W/mK)	0	0	0

Table 2 Convergence of the non-dimensional radial displacement of a single-layer rotating FG cylindrical shell ($t/R_o = 0.2,\ L/R_o = 1,\ R_o = 1,\ p = 1,\quad \eta = \xi = 0.5,\quad N_e = 1$)

N_z^e	$\Omega = 100$ (Rad/s)			$\Omega = 200$ (Rad/s)		
	$N_r^e = 13$	$N_r^e = 15$	$N_r^e = 17$	$N_r^e = 13$	$N_r^e = 15$	$N_r^e = 17$
7	53.2331	−76.0904	−62.6111	43.8146	−62.0881	−51.1706
9	0.5795	0.5928	0.4296	0.6977	0.7086	0.5749
11	0.6562	0.6567	0.6570	0.7605	0.7609	0.7612
13	0.6548	0.6573	0.6571	0.7594	0.7614	0.7613
15	0.6572	0.6566	0.6571	0.7613	0.7609	0.7613
17	0.6571	0.6572	0.6572	0.7613	0.7613	0.7613
19	0.6571	0.6572	0.6572	0.7613	0.7613	0.7613

Table 3 Convergence of the results for the three layered rotating cylindrical shell [model (I)] ($L/R_o = 1,\ R_o = 1,\ N_z^e = 25,\ N_e = 3,\ \eta = \xi = 0.5,\ p = 1$)

N_r^e	t/R_o	$\Omega = 100$ (Rad/s)				$\Omega = 200$ (Rad/s)			
		U	$\Sigma_{\theta\theta}$	Σ_{zz}	Σ_{rr}	U	$\Sigma_{\theta\theta}$	Σ_{zz}	Σ_{rr}
13	0.1	0.7560	−0.242	−0.149	−0.027	0.8813	−0.026	−0.122	−0.023
15		0.7562	−0.242	−0.149	−0.027	0.8814	−0.026	−0.122	−0.023
17		0.7562	−0.242	−0.149	−0.027	0.8814	−0.026	−0.122	−0.023
13	0.2	0.7022	−0.285	−0.124	−0.052	0.8034	−0.078	−0.102	−0.044
15		0.7020	−0.285	−0.124	−0.052	0.8032	−0.078	−0.102	−0.044
17		0.7020	−0.285	−0.124	−0.052	0.8032	−0.078	−0.102	−0.044

Table 4 Comparison of the results for the rotating FG annular disk subjected to non-uniform temperature rise [$R_i/R_o = 0.2, L/R_o = 0.05, \Omega = 600$ (Rad/s) , $R_o = 1, \eta = 0.5$]

n	ξ	Present			Analytic [9]		
		U	$\Sigma_{\theta\theta}$	Σ_{rr}	U	$\Sigma_{\theta\theta}$	Σ_{rr}
0.5	0	0.1813	0.3691	1.41E−4	0.1813	0.3689	0
	0.5	0.2546	0.1730	0.1290	0.2547	0.1735	0.1294
	1	0.4054	0.0101	−1.24E−4	0.4054	0.0102	0
0	0	0.1470	0.6675	−1.51E−4	0.1468	0.6680	0
	0.5	0.2381	0.1639	0.1583	0.2381	0.1636	0.1580
	1	0.3997	0.005	−3.62E−4	0.3994	4.73E−3	0
−0.5	0	0.1197	1.2163	−4.60E−4	0.1194	1.2152	0
	0.5	0.2267	0.1464	0.1891	0.2267	0.1465	0.1893
	1	0.3965	0.0021	−1.43E−5	0.3961	1.74E−3	0

where $\sigma_{ij}^e\ (i, j = r, \theta, z)$ are the stress tensor components; $C_{ij}^e \left[= C_{ij}^e\ (r, T^e)\ ; i, j = 1, 2, 3, 5\right]$ are the material elastic coefficients; ε_T^e is the thermal strain; $\alpha^e \left[= \alpha^e\ (r, T^e)\right]$ is the thermal expansion coefficient; and $\varepsilon_{ij}^e\ (i, j = r, \theta, z)$ are the strain tensor components, which are related to displacement components as

$$\varepsilon_{rr}^e = \frac{\partial u^e}{\partial r},\quad \varepsilon_{\theta\theta}^e = \frac{u^e}{r}, \varepsilon_{zz}^e = \frac{\partial w^e}{\partial z},\quad \underline{\varepsilon_{rz}^e = \frac{1}{2}\left(\frac{\partial u^e}{\partial z} + \frac{\partial w^e}{\partial r}\right).} \tag{7}$$

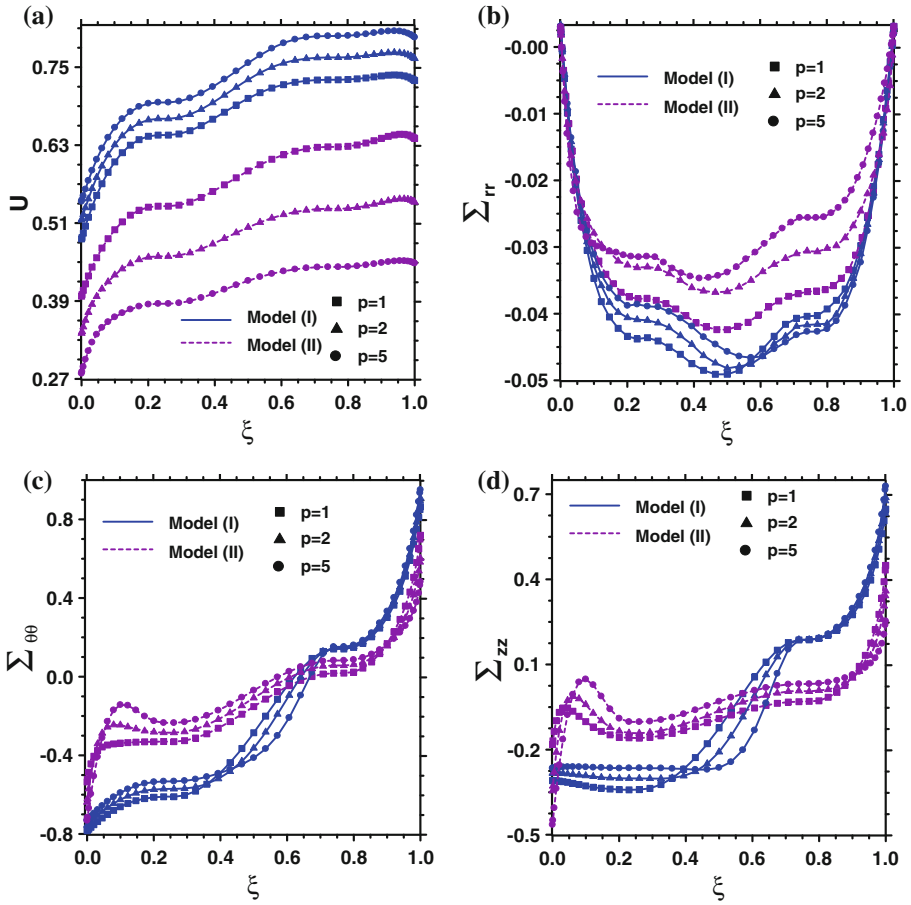

Fig. 2 The influence of power law index on the results for the free ends rotating three layered FG cylindrical shell $\left[t/R_o = 0.2, L/R_o = 1, R_o = 1, N_e = 3, N_z^e = 25, N_r^e = 15, \Omega = 100 \text{ (Rad/s)}, \eta = 0.5\right]$

Also, the material elastic coefficients C_{ij}^e for an isotropic material are related to Young's modulus (E) and Poisson's ratio (ν) by

$$C_{11}^e = C_{22}^e = C_{33}^e = \frac{(1-\nu^e)\,E^e}{(1+\nu^e)\,(1-2\nu^e)},\; C_{12}^e = C_{23}^e = C_{13}^e = \frac{\nu^e E^e}{(1+\nu^e)\,(1-2\nu^e)},\; C_{55}^e = \frac{E^e}{2\,(1+\nu^e)}. \quad (8.1\text{–}3)$$

Using Eqs. (7) and (8), the thermolelastic equilibrium equations in terms of the displacement components become

$$\begin{aligned}\delta u \;:\; & C_{11}^e \frac{\partial^2 u^e}{\partial r^2} + \left(\frac{dC_{11}^e}{dr} + \frac{C_{11}^e}{r}\right)\frac{\partial u^e}{\partial r} + C_{55}^e \frac{\partial^2 u^e}{\partial z^2} + \left(\frac{dC_{12}^e}{dr} - \frac{C_{22}^e}{r}\right)\frac{u^e}{r} \\ & + \left(\frac{dC_{13}^e}{dr} + \frac{C_{13}^e - C_{23}^e}{r}\right)\frac{\partial w^e}{\partial z} + \left(C_{55}^e + C_{13}^e\right)\frac{\partial^2 w^e}{\partial r \partial z} = \left(\frac{dC_{11}^e}{dr} + \frac{dC_{12}^e}{dr} + \frac{dC_{13}^e}{dr}\right)\alpha^e \Delta T^e \\ & + \left(C_{11}^e + C_{12}^e + C_{13}^e\right)\frac{d\left(\alpha^e \Delta T^e\right)}{dr} - \rho^e r \Omega^2, \end{aligned} \quad (9)$$

$$\begin{aligned}\delta w \;:\; & \left(C_{13}^e + C_{55}^e\right)\frac{\partial^2 u^e}{\partial r \partial z} + C_{55}^e \frac{\partial^2 w^e}{\partial r^2} + \left(\frac{dC_{55}^e}{dr} + \frac{C_{23}^e + C_{55}^e}{r}\right)\frac{\partial u^e}{\partial z} \\ & + C_{33}^e \frac{\partial^2 w^e}{\partial z^2} + \left(\frac{dC_{55}^e}{dr} + \frac{C_{55}^e}{r}\right)\frac{\partial w^e}{\partial r} = 0 \end{aligned} \quad (10)$$

where ρ^e is the mass density.

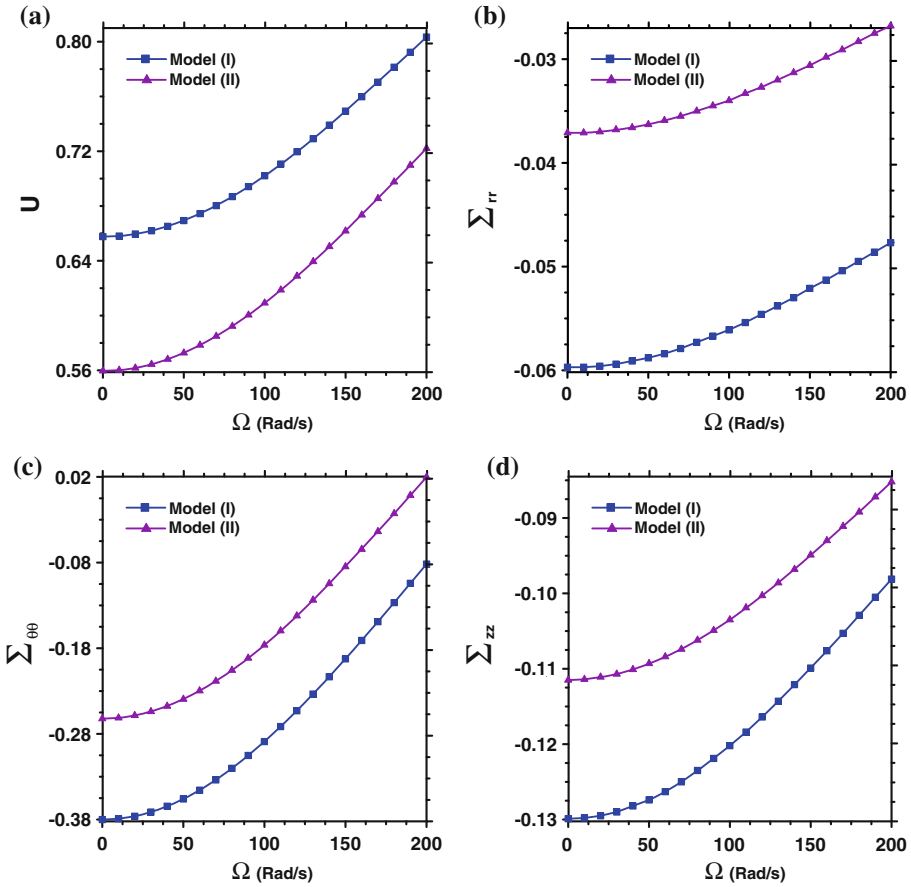

Fig. 3 The results for the free ends rotating three layered FG cylindrical shell $\left(t/R_{\mathrm{o}}=0.2, L/R_{\mathrm{o}}=1,\ R_{\mathrm{o}}=1,\ N_e=3,\ N_z^e=25,\ N_r^e=15,\ \eta=\xi=0.5\right)$

The external boundary conditions at the lower and upper surfaces $(z=0,\ L)$ of the shell are

$$\text{Either } u^e=0 \quad \text{or} \quad C_{55}^e\left(\frac{\partial u^e}{\partial z}+\frac{\partial w^e}{\partial r}\right)=0; \tag{11.1, 2}$$

$$\text{Either } w^e=0 \text{ or } \quad C_{13}^e\frac{\partial u^e}{\partial r}+\frac{C_{23}^e}{r}u^e+C_{33}^e\frac{\partial w^e}{\partial z}-\left(C_{13}^e+C_{23}^e+C_{33}^e\right)\alpha^e\Delta T^e=0. \tag{12.1, 2}$$

Also, at the inner and outer surfaces of the shell $\left(r=R_i^1,\ R_o^{N_e}\right)$, one has

$$C_{11}^e\frac{\partial u^e}{\partial r}+\frac{C_{12}^e}{r}u^e+C_{13}^e\frac{\partial w^e}{\partial z}-\left(C_{11}^e+C_{12}^e+C_{13}^e\right)\alpha^e\Delta T^e=0, \quad C_{55}^e\left(\frac{\partial u^e}{\partial z}+\frac{\partial w^e}{\partial r}\right)=0. \tag{13.1, 2}$$

The thermoelastic geometrical and natural compatibility conditions at the interface of two adjacent layers of the shell are as follows:

$$u^e\left(R_{\mathrm{o}}^e,z\right)=u^{e+1}\left(R_i^{e+1},z\right), \quad w^e\left(R_{\mathrm{o}}^e,z\right)=w^{e+1}\left(R_i^{e+1},z\right),$$
$$\left[C_{11}^e r\frac{\partial u^e}{\partial r}+C_{12}^e u^e+C_{13}^e r\frac{\partial w^e}{\partial z}-r\left(C_{11}^e+C_{12}^e+C_{13}^e\right)\alpha^e\Delta T^e\right]_{r=R_{\mathrm{o}}^e}$$

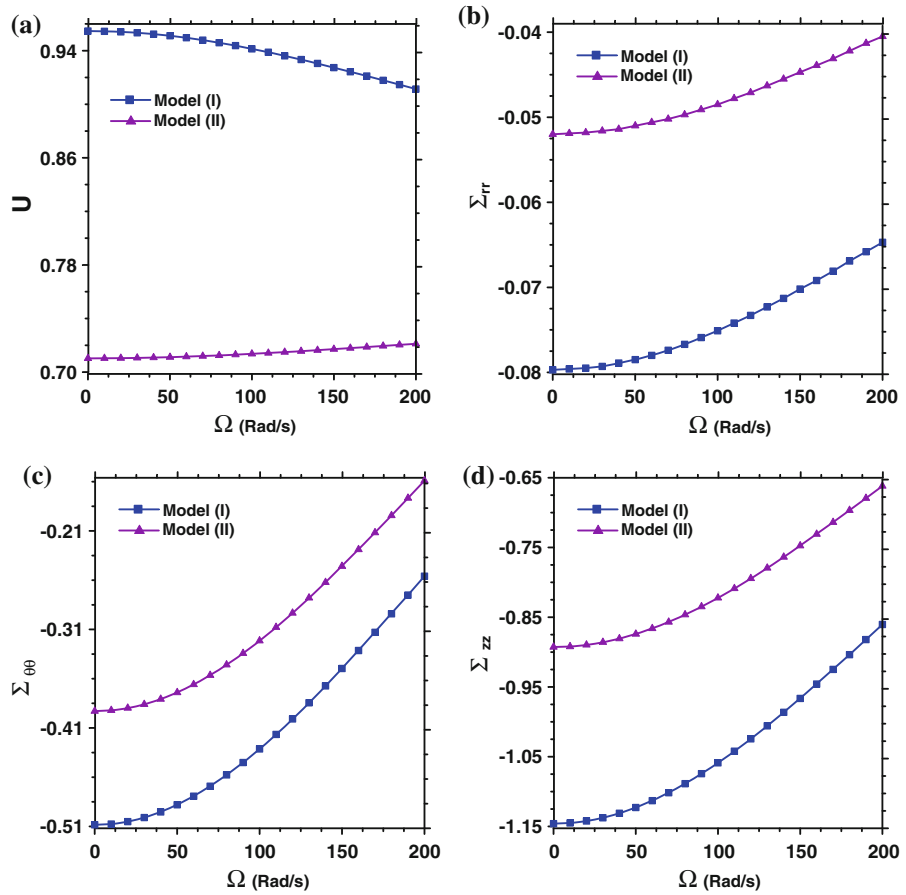

Fig. 4 The results for the clamped ends rotating three layered FG cylindrical shell ($t/R_o = 0.2, L/R_o = 1, R_o = 1, N_e = 3, N_z^e = 19, N_r^e = 11, \eta = \xi = 0.5$)

$$= \left[C_{11}^{e+1} r \frac{\partial u^{e+1}}{\partial r} + C_{12}^{e+1} u^{e+1} + C_{13}^{e+1} r \frac{\partial w^{e+1}}{\partial z} - r \left(C_{11}^{e+1} + C_{12}^{e+1} + C_{13}^{e+1} \right) \alpha^{e+1} \Delta T^{e+1} \right]_{r=R_i^{e+1}},$$

$$C_{55}^{e} \left(\frac{\partial u^{e}}{\partial z} + \frac{\partial w^{e}}{\partial r} \right)\Big|_{r=R_o^{e}} = C_{55}^{e+1} \left(\frac{\partial u^{e+1}}{\partial z} + \frac{\partial w^{e+1}}{\partial r} \right)\Big|_{r=R_i^{e+1}}. \quad (14.1\text{–}4)$$

In this study, it is assumed that the lower and upper surfaces of the shell ($z = 0$ and $z = L$) have different types of the classical boundary conditions, which can be obtained by combining the conditions stated in Eqs. (11) and (12) as follows:

$$\text{Simply support (S)}: u^e = 0, \quad C_{13}^{e} \frac{\partial u^{e}}{\partial r} + \frac{C_{23}^{e}}{r} u^{e} + C_{33}^{e} \frac{\partial w^{e}}{\partial z} - \left(C_{13}^{e} + C_{23}^{e} + C_{33}^{e} \right) \alpha^{e} \Delta T^{e} = 0, \quad (15.1, 2)$$

$$\text{Clamped (C)}: u^e = 0, w^e = 0, \quad (16.1, 2)$$

$$\text{Free (F)}: C_{55}^{e} \left(\frac{\partial u^{e}}{\partial z} + \frac{\partial w^{e}}{\partial r} \right) = 0, C_{13}^{e} \frac{\partial u^{e}}{\partial r} + \frac{C_{23}^{e}}{r} u^{e} + C_{33}^{e} \frac{\partial w^{e}}{\partial z} - \left(C_{13}^{e} + C_{23}^{e} + C_{33}^{e} \right) \alpha^{e} \Delta T^{e} = 0. \quad (17.1, 2)$$

If it is not impossible to solve the above system of differential equations, it may be very difficult to obtain such a solution. Hence, a numerical method should be used to solve this system of equations. On the other hand, the differential quadrature method (DQM) as an accurate and simple numerical method has been successfully employed for different structural problems, especially, for those with variable coefficients differential equations [14–19]. Hence, it will be used to discretize the thermal heat conduction as well as the governing

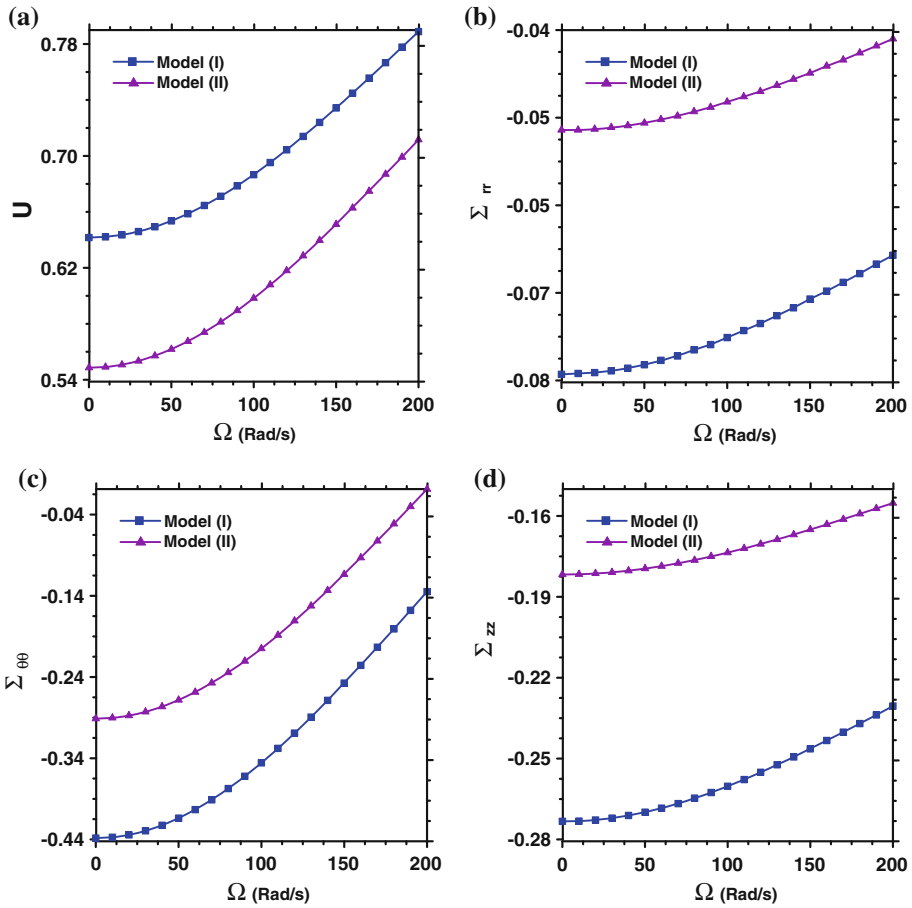

Fig. 5 The results for the simply supported rotating three layered FG cylindrical shell ($t/R_o = 0.2$, $L/R_o = 1$, $R_o = 1$, $N_e = 3$, $N_z^e = 19$, $N_r^e = 11$, $\eta = \xi = 0.5$)

differential equations of motion and the related boundary and compatibility conditions in each mathematical layer.

According to the DQM, in the computational domain, each mathematical layer is discretized into N_r^e and N_z^e discrete grid points along the r and z directions, respectively. At each domain grid point, the strong forms of the equations of motion and at boundary grid points, the boundary and the interface compatibility conditions are discretized using the DQ-discretization rules. For brevity purpose, here only the DQ discretized form of the heat conduction equation (3) for the eth layer is presented. At each domain grid point (i, j) with $i = 2, \ldots, \hat{N}_r^e \left(= N_r^e - 1\right)$ and $j = 2, \ldots, \hat{N}_z^e \left(= N_z^e - 1\right)$, one gets

$$K_i^e \sum_{m=1}^{N_r^e} B_{im}^{er} T_m^e + \left[\left(\frac{dK^e}{dr} \right)_i + \frac{K_i^e}{r_i} \right] \sum_{m=1}^{N_r^e} A_{im}^{er} T_m^e = 0 \tag{18}$$

where A_{ij}^{er} and B_{ij}^{er} represent the weighting coefficients of the first- and second-order derivatives along the r direction, respectively [14–19]. The cosine-type grid generation rule is used in both the r and z directions [14–19]. In a similar manner, the other differential equations, the external boundary and the interface compatibility conditions, can be discretized. After discretizing these equations, one obtains a system of algebraic equations. Solving it, the temperature distribution together with the displacement and stress components is obtained.

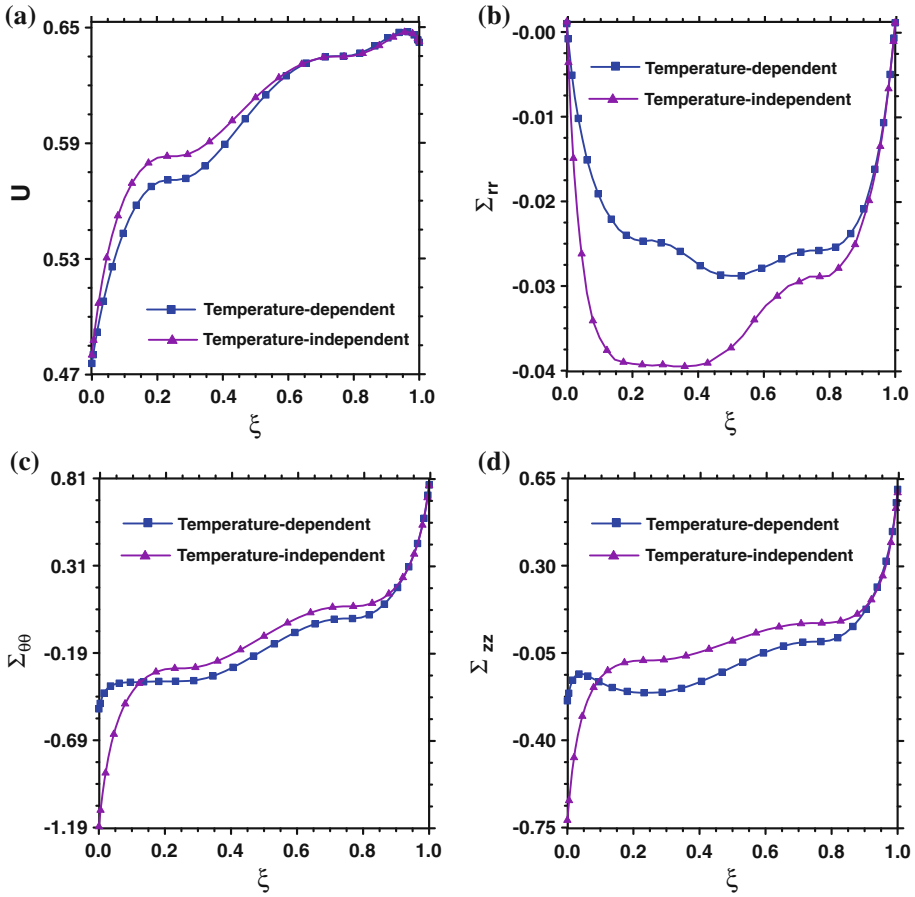

Fig. 6 The results for the free ends rotating shell [model (II)] with the temperature-dependent/independent material properties $\left[t/R_{\mathrm{o}} = 0.2,\ L/R_{\mathrm{o}} = 1,\ R_{\mathrm{o}} = 1,\ p = 1,\ \eta = 0.5,\ N_e = 3,\ N_z^e = 19,\ N_r^e = 15,\ \Omega = 100\ (\mathrm{Rad/s})\right]$

3 Numerical results

In this section, firstly, the fast rate of convergence and the accuracy of the method for the thermoelastic analysis of rotating FG laminated cylindrical shells are investigated. Then, a parametric study for two common types of FG sandwich shells, namely, the sandwich with homogeneous inner/outer layers and FG core [model (I), see Fig. 1a] and the sandwich with FG inner/outer layers and homogeneous core [model (II), see Fig. 1b] is presented. Otherwise specified, the material properties are assumed to be temperature dependent and vary according to power law distribution; (1) also, the non-dimensional parameters are defined as:

$$\eta = z/L, \quad \xi = \frac{r - R_i}{R_{\mathrm{o}} - R_i}, \quad U = \frac{u E_c}{(1+\nu_c)\left[E_c\alpha_c T_c + (1-\nu_c)\,\rho_c\Omega^2 R_o^2\right] R_o},$$
$$\Sigma_{ii} = \frac{(1-\nu_c)\,\sigma_{ii}}{E_c\alpha_c T_c + (1-\nu_c)\,\rho_c\Omega^2 R_o^2}\ (i = r, \theta, z) \tag{19}$$

where L is the length of the cylindrical shell. Also, otherwise specified, the values of $T_0 = 300\,(\mathrm{K})$, $T_\infty = 1{,}100\,(\mathrm{K})$ and $h = 200\,\left(\mathrm{W/m^2K}\right)$ are used in all examples.

The material properties of Ti-6Al-4V and ZrO_2, as given in Table 1, are used to obtain the new numerical results, which are chosen from the work of Kim [20]. They are valid for the temperature range of $300\ \mathrm{K} \le T \le 1{,}100\ \mathrm{K}$.

As a first example, the convergence behavior of the non-dimensional radial displacement component of a single-layer rotating FG cylindrical shell against the numbers of grid points along the r and z directions is shown in Table 2. Also, the convergence behavior of the method for the rotating shell of model (I) is presented in Table 3. In all cases, the fast rate of convergence of the method is quite evident.

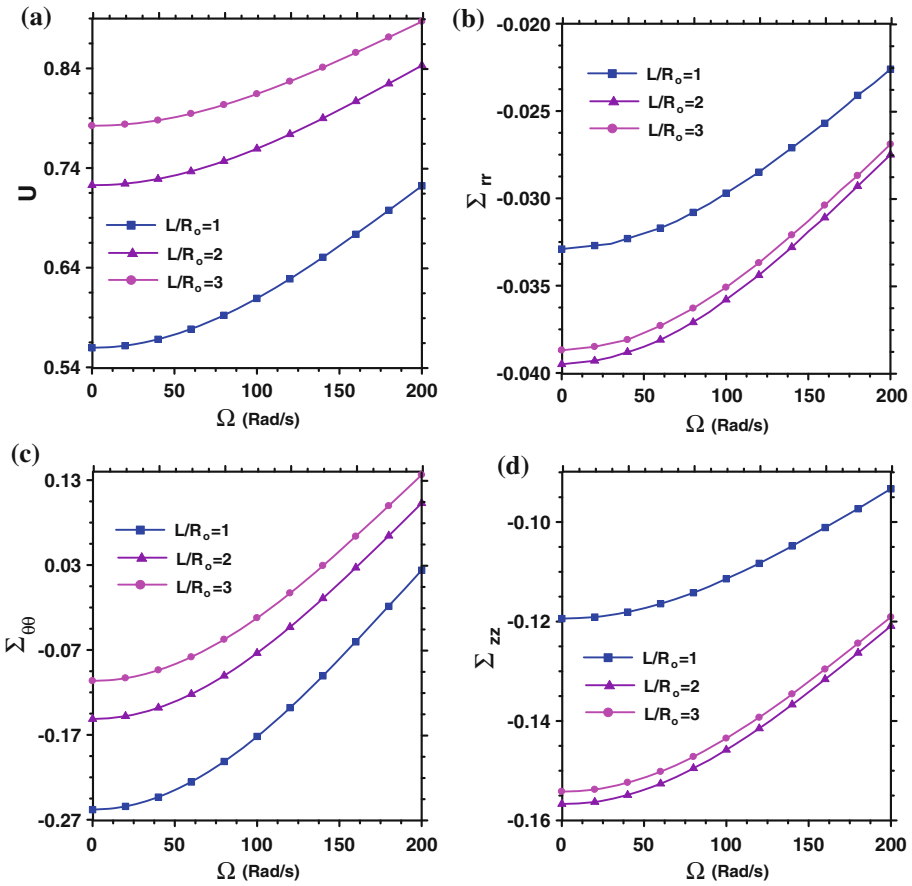

Fig. 7 The influences of length-to-outer radius ratio on the results for the free ends rotating shell (model II) ($t/R_o = 0.2$, $R_o = 1$, $p = 1$, $N_e = 3$, $N_z^e = 35$, $N_r^e = 15$, $\eta = \xi = 0.5$)

Due to the lack of numerical results for rotating FG cylindrical shells in thermal environment, the results for an annular disk as a limiting case of a cylinder (cylinder with small length-to-outer radius ratio) is used to verify the presented approach. For this purpose, the numerical results for a rotating FG annular disk subjected to thermal environment are compared with the analytical solution of Peng and Li [9] in Table 4. They transformed the one-dimensional thermoelasticity equation into a Fredholm integral equation to obtain the analytical solution. To find such a solution, all the material properties, except Poisson's ratio, were assumed to vary according to $\psi = \psi_0 r^n$ where ψ_0 is a material constant at the outer surface and n is the material graded index. The material properties are as follows [9]:

$$E_m = 70 \text{ GPa}, \nu_m = 0.3, K_m = 209 \ \left(\text{W/m°C}\right), \alpha_m = 23 \times 10^{-6} \ \left(1/°\text{C}\right), \rho_m = 2{,}700 \ \left(\text{Kg/m}^3\right),$$
$$E_c = 151 \text{ GPa}, \nu_c = 0.3, K_c = 2 \ \left(\text{W/m°C}\right), \alpha_c = 10 \times 10^{-6} \ \left(1/°\text{C}\right), \rho_c = 5{,}700 \ \left(\text{Kg/m}^3\right).$$

Also the surface temperatures at the inner and outer surfaces of disk are assumed to be

$$T\left(R_i\right) = 0°\text{C}, \quad T\left(R_o\right) = 1{,}000°\text{C}.$$

The non-dimensional radial displacement and stress components at different locations and for different values of the material graded index (n) are compared with those of Peng and Li [9]. Excellent agreement between the results of the two approaches can be seen.

After validating the presented approach, some parametric study for FG rotating cylindrical shells subjected to thermal environment is performed. As a first example, a comparison between the results of the two shell models (I) and (II) with free ends is performed in Fig. 2. The effects of different values of the material graded

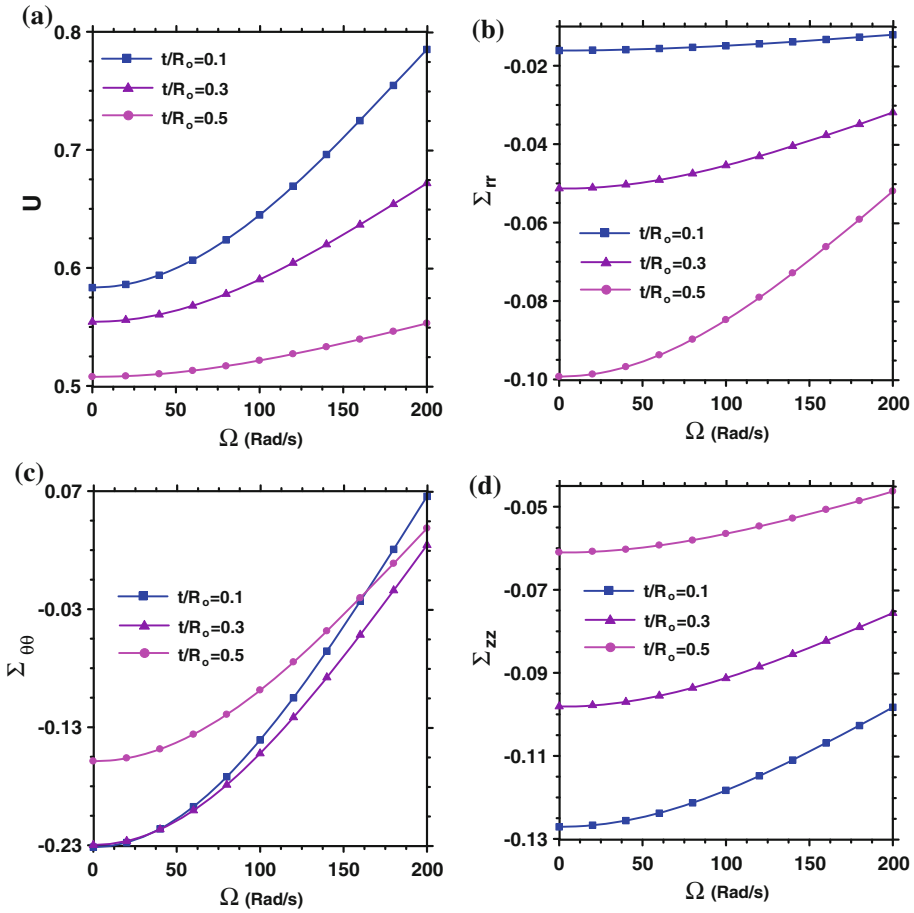

Fig. 8 The influence of thickness-to-outer radius ratio on the results for the free ends rotating shell (model II) ($L/R_o = 1$, $R_o = 1$, $p = 1$, $N_e = 3$, $N_z^e = 27$, $N_r^e = 19$, $\eta = \xi = 0.5$)

index (p) on the results are shown in this figure. It can be seen that the material graded index significantly affects the non-dimensional radial displacement component of model II.

The influence of the angular velocity on the results of the two shell models (I) and (II) with three different sets of end boundary conditions is shown in Figs. 3, 4, and 5. The results for the FG rotating shells with both ends free, clamped and simply supported are presented in Figs. 3, 4, and 5, respectively. It can be seen that increasing the angular velocity, the non-dimensional parameters increase for all types of boundary conditions, except the non-dimensional radial displacement for the shells with clamped boundary condition.

The effects of temperature dependence of material properties on the results for the free ends rotating shell of model (II) are shown in Fig. 6. It can be seen that the temperature dependence of material properties has a significant effect on the stress components and cannot be ignored. Also, it is observable that its influence on the radial displacement component is less than on the stress components.

The influences of the length-to-outer radius and thickness-to-length ratios for the free ends rotating shell of model (II) are presented in Figs. 7 and 8, respectively. From Fig. 7, it can be seen that the length-to-outer radius ratio has a significant effect on the results of the free ends shell. Also, it is observable from Fig. 8 that increasing the thickness-to-outer radius ratio, the radial stress and displacement components increase but the axial stress component reduces. In addition, it is obvious that with increasing the angular velocity the non-dimensional parameter increases for all values of the thickness-to-outer radius ratio.

As an important thermal parameter, the influence of the convective heat transfer coefficient on the results of the free ends rotating shell of model (II) is presented in Fig. 9. It is obvious that this parameter considerably changes the stress and displacement variations in the shell especially for the values of $h \leq 100(\mathrm{W/m^2K})$.

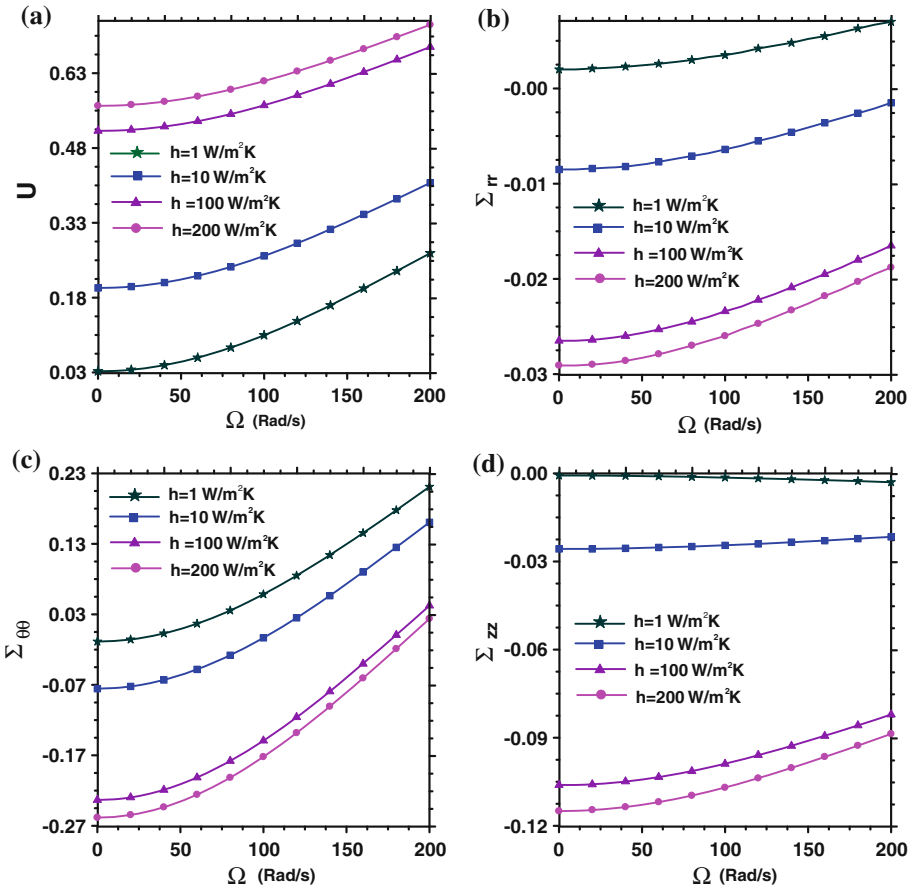

Fig. 9 The influence of convection heat transfer coefficient on the results for the free ends rotating shell of model (II) ($t/R_o = 0.2$, $L/R_o = 1$, $R_o = 1$, $p = 1$, $N_e = 3$, $N_z^e = 25$, $N_r^e = 15$, $\eta = \xi = 0.5$)

4 Conclusion

Using the elasticity-based layerwise approach, the thermoelastic analysis of rotating laminated functionally graded (FG) cylindrical shells in thermal environment was performed. The material properties were assumed to be temperature dependent and graded in the thickness direction. In order to accurately model the laminated shell, it was divided into a set of mathematical layers. Then, the differential quadrature method (DQM), as an efficient and accurate numerical method, was employed to discretize the thermal and thermo-mechanical governing differential equations of each layer together with the related end boundary conditions and compatibility conditions at the interface of two adjacent layers. The convective boundary condition on the inner surface and the constant temperature on the outer surface of the shell were assumed. The convergence behavior of the method was numerically demonstrated, and comparison studies with the available solutions in the literature were performed to validate the presented formulation and the method of solution. Then, parametric studies were performed to study the behavior of two commonly used laminated FG shells. From the obtained results, it was concluded that the temperature dependence of material properties, material graded index, the convective heat transfer coefficient, the angular velocity, the length-to-outer radius, and the thickness-to-outer radius ratios have significant effects on the displacement and stress components of the FG laminated cylindrical shell.

References

1. Ding, H.J., Wang, H.M., Chen, W.Q.: A solution of a non-homogeneous orthotropic cylindrical shell for axisymmetric plane strain dynamic thermoelastic problems. J. Sound Vib. **263**, 815–829 (2003)
2. Pelletier, J.L., Vel, S.S.: An exact solution for the steady-state thermoelastic response of functionally graded orthotropic cylindrical shells. Int. J. Solids Struct. **43**, 1131–1158 (2006)

3. Zhao, X., Lee, Y.Y., Liew, K.M.: Thermoelastic and vibration analysis of functionally graded cylindrical shells. Int. J. Mech. Sci. **51**, 694–707 (2009)
4. Bayat, M., Saleem, M., Sahari, B.B., Hamouda, A.M.S., Mahdi, E.: Thermoelastic analysis of a functionally graded rotating disk with small and large deflections. Thin-Walled Struct. **45**, 677–691 (2007)
5. Hosseini Kordkheili, S.A., Naghdabadi, R.: Thermoelastic analysis of a functionally graded rotating disk. Compos. Struct. **79**, 508–516 (2007)
6. Bayat, M., Sahari, B.B., Saleem, M., Aidy, A., Wong, S.V.: Thermoelastic solution of a functionally graded variable thickness rotating disk with bending based on the first-order shear deformation theory. Thin-Walled Struct. **47**, 568–582 (2009)
7. Bayat, M., Saleem, M., Sahari, B.B., Hamouda, A.M.S., Mahdi, E.: Mechanical and thermal stresses in a functionally graded rotating disk with variable thickness due to radially symmetry loads. Int. J. Press. Vess. Pip. **86**, 357–372 (2009)
8. Bayat, M., Sahari, B.B., Saleem, M., Hamouda, A.M.S., Reddy, J.N.: Thermoelastic analysis of functionally graded rotating disks with temperature-dependent material properties: uniform and variable thickness. Int. J. Mech. Mater. Des. **5**, 263–279 (2009)
9. Peng, X.L., Li, X.F.: Thermal stress in rotating functionally graded hollow circular disks. Compos. Struct. **92**, 1896–1904 (2010)
10. Nie, G.J., Batra, R.C.: Stress analysis and material tailoring in isotropic linear thermoelastic incompressible functionally graded rotating disks of variable thickness. Compos. Struct. **92**, 720–729 (2010)
11. Zenkour, A.M., Elsibai, K.A., Mashat, D.S.: Elastic and viscoelastic solutions to rotating functionally graded hollow and solid cylinders. Appl. Math. Mech. **29**, 1601–1616 (2008)
12. Zamani Nejad, M., Rahimi, G.H.: Elastic analysis of FGM rotating cylindrical pressure vessels. J. Chin. Inst. Eng. **33**, 525–530 (2010)
13. Khorshidvand, A.R., Khalili, S.M.R.: A new analytical solution for deformation and stresses in functionally graded rotating cylinder subjected to thermal and mechanical loads. In: International Conference on Continuum Mechanics (5TH IASME-WSEAS), pp. 201–204 (2010)
14. Malekzadeh, P.: Two-dimensional in-plane free vibrations of functionally graded circular arches with temperature-dependent properties. Compos. Struct. **91**, 38–47 (2009)
15. Sobhani Aragh, B., Yas, M.H.: Static and free vibration analyses of continuously graded fiber-reinforced cylindrical shells using generalized power-law distribution. Acta Mech. **215**, 155–173 (2010)
16. Malekzadeh, P., Shahpari, S.A., Ziaee, H.R.: Three-dimensional free vibration of thick functionally graded annular plates in thermal environment. J. Sound Vib. **329**, 425–442 (2010)
17. Zahedinejad, P., Malekzadeh, P., Farid, M., Karami, G.: A semi-analytical three-dimensional free vibration analysis of functionally graded curved panels. Int. J. Press. Vess. Pip. **87**, 470–480 (2010)
18. Malekzadeh, P.: Three-dimensional free vibration analysis of thick functionally graded plates on elastic foundations. Compos. Struct. **89**, 367–373 (2009)
19. Malekzadeh, P.: Three-dimensional thermal buckling analysis of functionally graded arbitrary straight-sided quadrilateral plates using differential quadrature method. Compos. Struct. **93**, 1246–1254 (2011)
20. Kim, Y.W.: Temperature dependent vibration analysis of functionally graded rectangular plates. J. Sound Vib. **284**, 531–549 (2005)